Gaussianity and Isotropy analyses on Planck data

P. Vielva, on behalf of the Planck Collaboration

CosmoRENATA, Valencia, 3rd June 2013

Gaussianity and Isotropy Planck Papers

Planck 2013 results
XXIV

Constraints on primordial non-Gaussianity

Planck 2013 results
XXV

Searches for cosmic strings and other topological deffects

Planck 2013 results
XXIII

Isotropy and statistics of the CMB

Planck 2013 results
XIX

The integrated Sachs-Wolfe effect

Planck 2013 results
XXVI

Background geometry and topology of the Universe

Gaussianity and Isotropy Planck Papers

The scope is to test the Gaussianity and statistical isotropy of the CMB, as expected from the standard cosmological scenario

Testing these fundamental properties is crucial for:

- validating the **standard cosmological scenario**
- understanding the physical nature of the Universe and the **initial conditions of structure formation**
- providing support to the common **assumptions usually made** in the power spectrum estimation and the cosmological parameters determination

Significant **deviations** of Gaussianity and isotropy **are expected**, e.g., non-linear process that lead to secondary anisotropies as **the ISW-lensing correlation**.

It also provides **insights on some anomalies previously claimed on WMAP data**

Gaussianity and Isotropy Planck Papers

Most of the analyses have been extensively tested against systematics introduced by foreground residuals:

The 4 clean CMB maps provided by Planck were analysed: Commander-Ruler (parametric in real space, SNR=1 @ l=1550), NILC (non-parametric in wavelet space, SNR=1 @ l =1790), SEVEM (non-parametric in real space, SNR=1 @ l=1790) and SMICA (semi-parametric in harmonic space, SNR=1 @ l=1790)

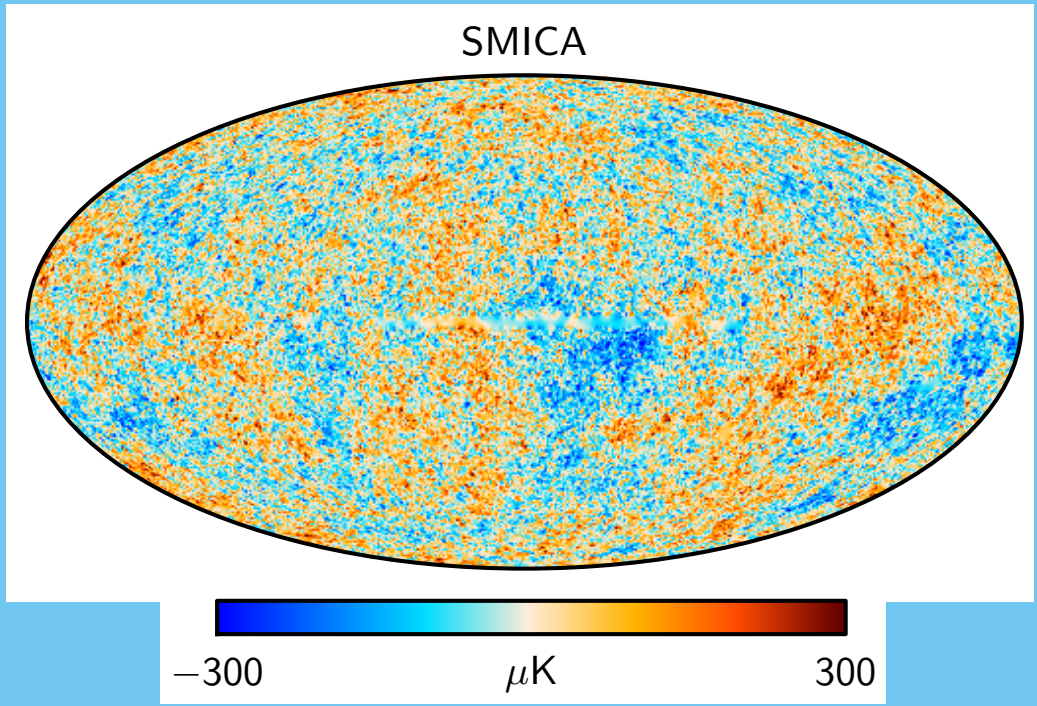

Gaussianity and Isotropy Planck Papers

Most of the analyses have been thoroughly tested against systematics introduced by foreground residuals:

- The **raw maps** at 70GHz, 100GHz, 143GHz and 217GHz
- The **clean maps** at 70GHz, 100GHz, 143GHz and 217GHz produced by **SEVEM**

- Corresponding **CMB and noise simulations** (FFP6):
  - including lensing
  - instrumental error propagated from the frequency channels
  - beam propagated from in flight main beams measurements

- A suite of **galactic masks**, including those used for the Planck likelihood

Isotropy and statistics of the CMB

A* suite *of non-parametric tools

Frequentist statistics:

- Among others, the 1-pdf, the N-point correlation function, and the wavelet moments have been applied to the data.
- A statistical quantity (e.g., a χ^2) has been defined and confronted against coherent simulations

Assessing the CMB anomalies

Frequentist and parametric statistics:

- Probing claimed WMAP anomalies on the Planck data (also related to some features highlighted by the previous tests)
- Establishing the significance is a difficult aspect, since many of the test are *a posteriori* analyses

Isotropy and statistics of the CMB

A suite of non-parametric tools

The 1-pdf

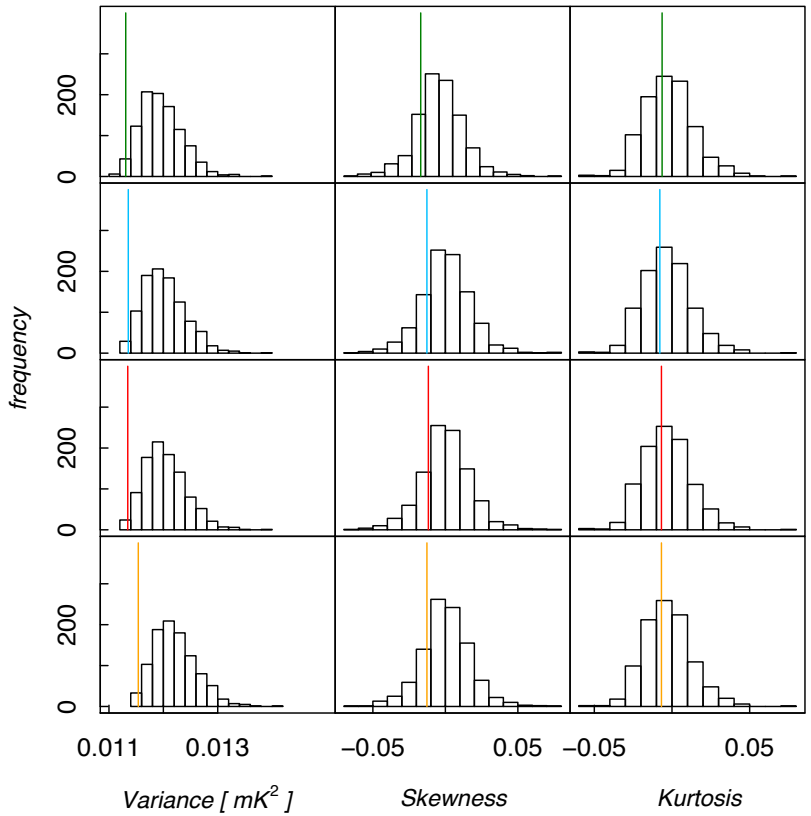

Fig. 1. Variance, skewness and kurtosis for the combined map of the four different component separation methods. From top row to bottom row C-R, NILC, SEVEM, SMICA.

Table 2. Lower tail probablity for the variance, skewness and kurtosis estimators at $N_{\rm side} = 2048$, using the U73 mask and four different component separation methods.

Method	Variance	Skewness	Kurtosis
C-R	0.021	0.189	0.416
NILC	0.020	0.191	0.392
SEVEM	0.014	0.206	0.419
SMICA	0.017	0.189	0.419

Table 3. Lower tail probablity for the variance, skewness and kurtosis estimators at $N_{\rm side} = 2048$, for the SMICA method, using different masks.

Mask	Variance	Skewness	Kurtosis
U73, $f_{\rm sky}$ =73%	0.017	0.189	0.419
CL58, $f_{\rm sky}$ =58%	0.003	0.170	0.363
CL37, $f_{\rm sky}$ =37%	0.030	0.314	0.266
Ecliptic North, $f_{\rm sky}$ =36%	0.001	0.553	0.413
Ecliptic South, $f_{\rm sky}$ =37%	0.483	0.077	0.556

Relation with the low variance (e.g., Cruz et al. 2011) and hemispherical asymmetry (e.g., Hansen 2004) anomalies

Isotropy and statistics of the CMB

A* suite *of non-parametric tools

The N-point correlation function

For an isotropic field, the N-point correlation function computed as averages over pixels **forming a given polynomial shape, do not depend neither of the position of the shape nor on its orientation.**

$$C_N(\theta_1,\ldots,\theta_{2N-3}) = \frac{\sum_i \left(w_1^i \cdots w_N^i\right)\left(\Delta T_1^i \cdots \Delta T_N^i\right)}{\sum_i w_1^i \cdots w_N^i}$$

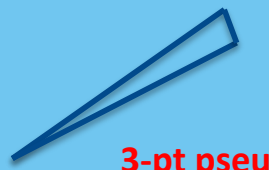

3-pt pseudo-collapsed

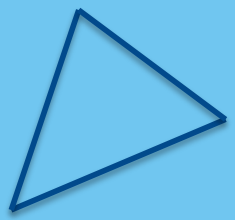

3-pt equilateral

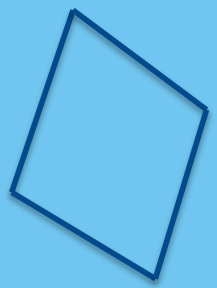

4-pt rhombic

There are many polynomial that can be analysed, but we concentrate in three (plus the 2-point correlation function) of them

Isotropy and statistics of the CMB

A suite of non-parametric tools

The N-point correlation function

Table 11. Probabilities of obtaining values of the χ^2 statistic of the N-point functions shown in Fig. 9 for the *Planck* fiducial ΛCDM model at least as large as the observed values of the statistic for *Planck* CMB maps with resolution parameter $N_{\rm side} = 2048$ estimated using the C-R, NILC, SEVEM, and SMICA methods.

	C-R	NILC	SEVEM	SMICA
2-pt.	0.335	0.474	0.573	0.497
pseudo-coll. 3-pt. . . .	0.522	0.463	0.469	0.448
equil. 3-pt.	0.853	0.789	0.819	0.796
4-pt.	0.532	0.534	0.579	0.526

Table 9. Probabilities of obtaining values for the χ^2 statistic of the *N*-point functions shown in Fig. 6 for the *Planck* fiducial ΛCDM model at least as large as the observed values of the statistic for the *Planck* CMB maps with resolution parameter $N_{\rm side} = 64$ estimated using the C-R, NILC, SEVEM and SMICA methods.

	C-R	NILC	SEVEM	SMICA
2-pt.	0.883	0.859	0.884	0.855
pseudo-coll. 3-pt. . . .	0.922	0.918	0.945	0.908
equil. 3-pt.	0.962	0.966	0.978	0.968
4-pt.	0.975	0.977	0.979	0.977

No evidence of statistical deviations from simulations.

More tension at largest scales and, in particular, for the **4-point rhombic function**.

However (as it will be shown latter), there is evidence of hemispherical asymmetry.

Isotropy and statistics of the CMB

A suite of non-parametric tools

Wavelet statistics

$$\omega_T(R,p) = \sum_{\ell=0}^{\ell_{\max}} \sum_{m=-\ell}^{m=\ell} t_{\ell m} W_\ell^{\mathrm{SMHW}}(R)\, Y_{\ell m}(p) \qquad t_{\ell m} = \int \mathrm{d}\Omega Y^*_{\ell m}(p)\, T(p)$$

Spherical Mexican Hat Wavelet coefficients

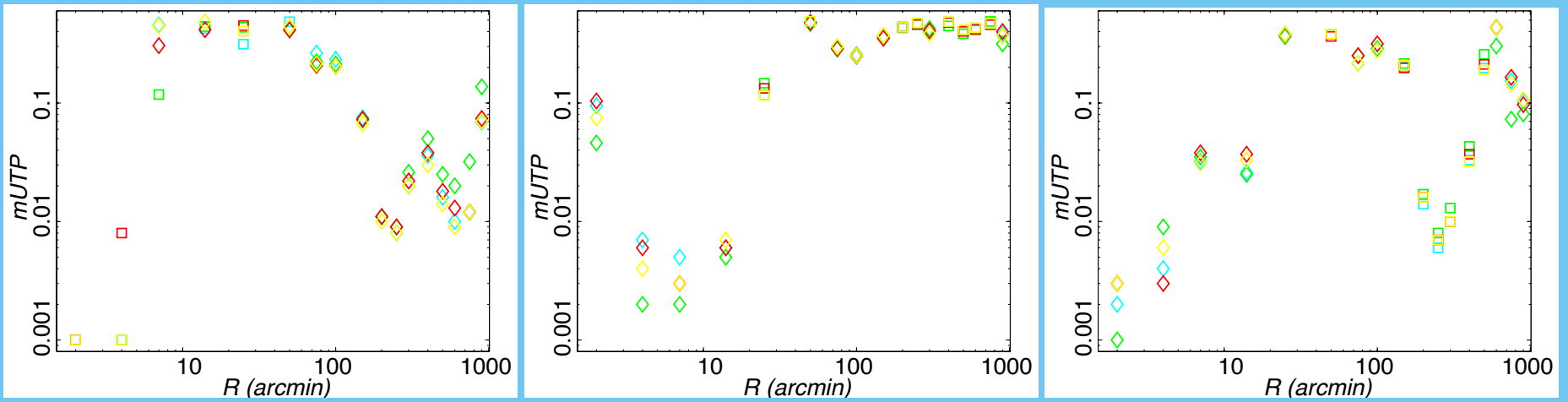

Fig. 13. Standard deviation (left), skewness (centre) and kurtosis (right) of the SMHW coefficients as a function of the wavelet scale *R*. Results are given for the four *Planck* CMB maps (green: `Commander-Ruler`, light-blue: `NILC`; red: `SEVEM`; yellow: `SMICA`). Modified upper tail probabilities (*mUTP*, see text for details) are obtained by comparing with 1000 simulations processed through the component separation pipelines. Squares represent modified upper tail probabilities that correspond to an actual upper tail probability above 0.5; diamonds represent upper tail probabilities below 0.5.

Isotropy and statistics of the CMB

A suite of non-parametric tools

Wavelet statistics

$$\omega_T(R,p) = \sum_{\ell=0}^{\ell_{\max}} \sum_{m=-\ell}^{m=\ell} t_{\ell m} W_\ell^{\mathrm{SMHW}}(R)\, Y_{\ell m}(p) \qquad t_{\ell m} = \int \mathrm{d}\Omega Y^*_{\ell m}(p)\, T(p)$$

Spherical Mexican Hat Wavelet coefficients

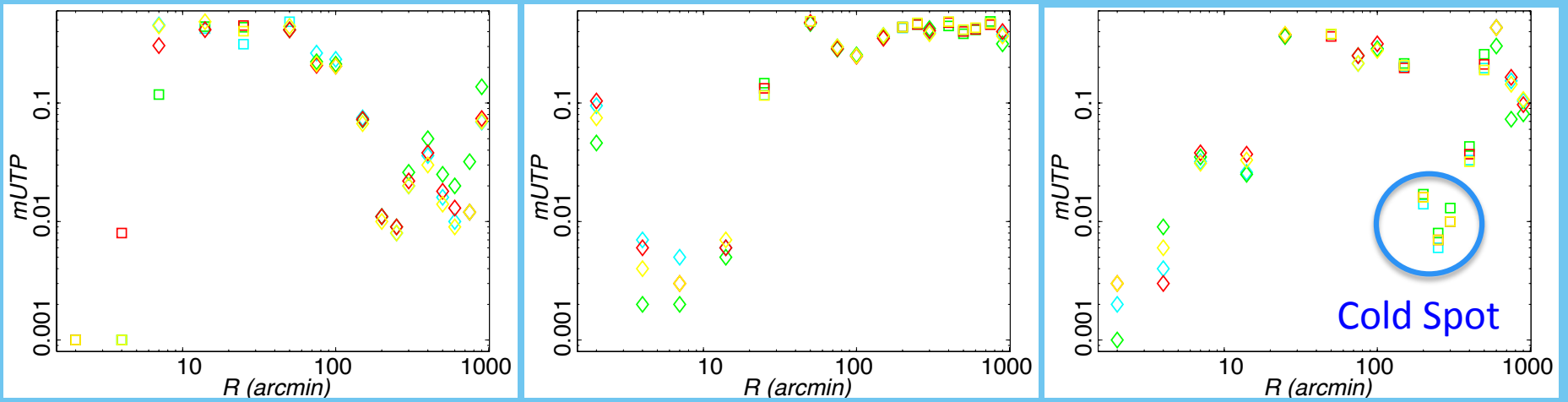

Fig. 13. Standard deviation (left), skewness (centre) and kurtosis (right) of the SMHW coefficients as a function of the wavelet scale R. Results are given for the four *Planck* CMB maps (green: `Commander-Ruler`, light-blue: `NILC`; red: `SEVEM`; yellow: `SMICA`). Modified upper tail probabilities (*mUTP*, see text for details) are obtained by comparing with 1000 simulations processed through the component separation pipelines. Squares represent modified upper tail probabilities that correspond to an actual upper tail probability above 0.5; diamonds represent upper tail probabilities below 0.5.

Isotropy and statistics of the CMB

A suite of non-parametric tools

Wavelet statistics

$$\omega_T(R,p) = \sum_{\ell=0}^{\ell_{\max}} \sum_{m=-\ell}^{m=\ell} t_{\ell m} W_\ell^{\mathrm{SMHW}}(R)\, Y_{\ell m}(p) \qquad t_{\ell m} = \int \mathrm{d}\Omega Y^*_{\ell m}(p)\, T(p)$$

Spherical Mexican Hat Wavelet coefficients

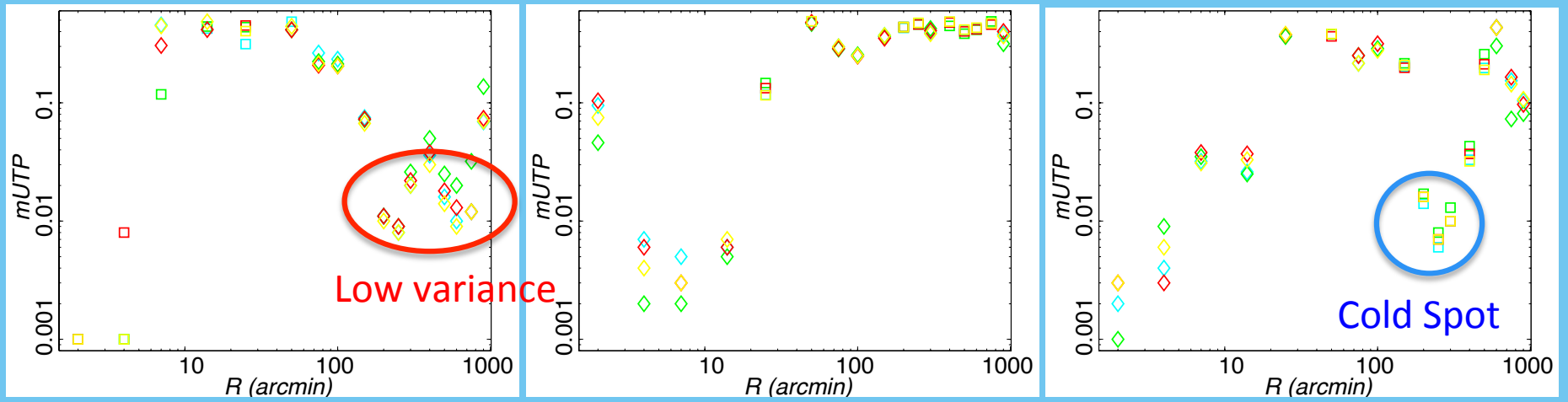

Fig. 13. Standard deviation (left), skewness (centre) and kurtosis (right) of the SMHW coefficients as a function of the wavelet scale R. Results are given for the four *Planck* CMB maps (green: `Commander-Ruler`, light-blue: `NILC`; red: `SEVEM`; yellow: `SMICA`). Modified upper tail probabilities (*mUTP*, see text for details) are obtained by comparing with 1000 simulations processed through the component separation pipelines. Squares represent modified upper tail probabilities that correspond to an actual upper tail probability above 0.5; diamonds represent upper tail probabilities below 0.5.

Isotropy and statistics of the CMB

A suite of non-parametric tools

Wavelet statistics

$$\omega_T(R,p) = \sum_{\ell=0}^{\ell_{\max}} \sum_{m=-\ell}^{m=\ell} t_{\ell m} W_\ell^{\mathrm{SMHW}}(R)\, Y_{\ell m}(p) \qquad t_{\ell m} = \int \mathrm{d}\Omega Y^*_{\ell m}(p)\, T(p)$$

Spherical Mexican Hat Wavelet coefficients

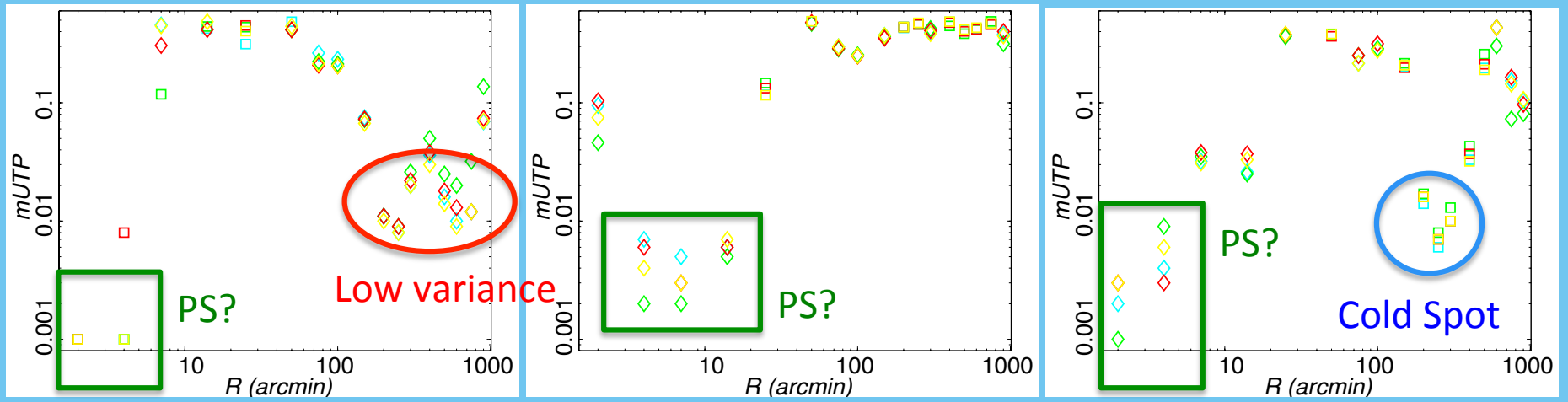

Fig. 13. Standard deviation (left), skewness (centre) and kurtosis (right) of the SMHW coefficients as a function of the wavelet scale R. Results are given for the four *Planck* CMB maps (green: `Commander-Ruler`, light-blue: `NILC`; red: `SEVEM`; yellow: `SMICA`). Modified upper tail probabilities (*mUTP*, see text for details) are obtained by comparing with 1000 simulations processed through the component separation pipelines. Squares represent modified upper tail probabilities that correspond to an actual upper tail probability above 0.5; diamonds represent upper tail probabilities below 0.5.

Isotropy and statistics of the CMB

Assessing the CMB anomalies

Multipole alignment

The direction of a given multipole is estimated by maximizing its angular momentum (e.g., de Oliveira-Costa et al. 2004) ➔ axes determination (headless vector)

The **quadrupole / octopole alignment in Planck data is within 9 degrees** (as compared to the 3 degrees reported in WMAP 9yr), and is **less significant** (approx 3%).

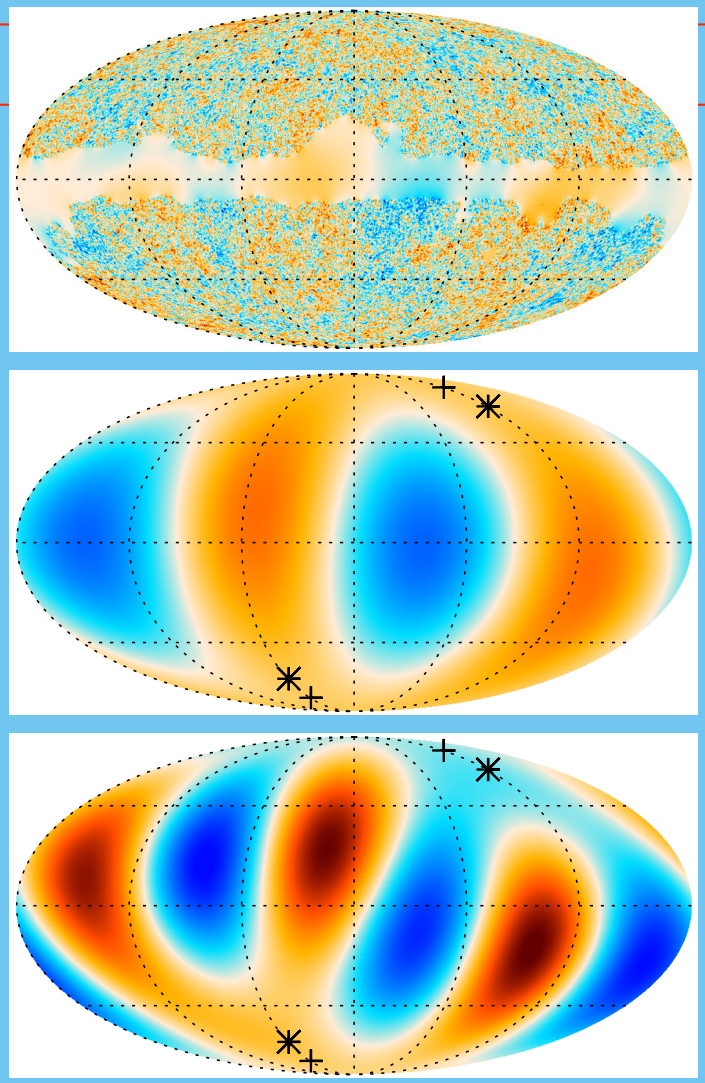

SMICA inpainted

quadrupole

octopole

Fig. 20. Upper: The Wiener filtered SMICA CMB sky (temperature range ± 400 μK). Middle: the derived quadrupole (temperature range ± 35 μK). Lower: the derived octopole (temperature range ± 35 μK). Cross and star signs indicate axes of the quadrupole and octopole, respectively, around which the angular momentum dispersion is maximized.

Isotropy and statistics of the CMB

Assessing the CMB anomalies

Low variance and hemispherical asymmetry

Table 18. Lower tail probablity for the variance, skewness and kurtosis at $N_{side} = 16$, using different masks.

Mask	C-R	NILC	SEVEM	SMICA
		Variance		
U73, $f_{sky} = 78\%$	0.019	0.017	0.014	0.019
CL58, $f_{sky} = 58\%$	0.004	0.003	0.003	0.003
CL37, $f_{sky} = 37\%$	0.028	0.017	0.018	0.016
Ecliptic North, $f_{sky} = 39\%$	0.001	0.001	0.001	0.002
Ecliptic South, $f_{sky} = 39\%$	0.464	0.479	0.454	0.490
		Skewness		
U73, $f_{sky} = 78\%$	0.016	0.015	0.023	0.012
CL58, $f_{sky} = 58\%$	0.208	0.139	0.162	0.147
CL37, $f_{sky} = 37\%$	0.517	0.467	0.503	0.469
Ecliptic North, $f_{sky} = 39\%$	0.502	0.526	0.526	0.521
Ecliptic South, $f_{sky} = 39\%$	0.004	0.006	0.008	0.004
		Kurtosis		
U73, $f_{sky} = 78\%$	0.972	0.973	0.966	0.982
CL58, $f_{sky} = 58\%$	0.630	0.726	0.711	0.711
CL37, $f_{sky} = 37\%$	0.069	0.135	0.130	0.124
Ecliptic North, $f_{sky} = 39\%$	0.094	0.229	0.196	0.245
Ecliptic South, $f_{sky} = 39\%$	0.933	0.916	0.886	0.948

As already seen in WMAP data, the **variance of the data is lower than expected**.

In addition, **large scale** analysis shows that also the **skewness** (and, at less extend the kurtosis), **also exhibit an anomalous behaviour**.

Even more, **these quantities are also sensible to the hemispherical asymmetry**, expressed in terms of the Ecliptic plane.

Isotropy and statistics of the CMB

Assessing the CMB anomalies

Low variance and hemispherical asymmetry

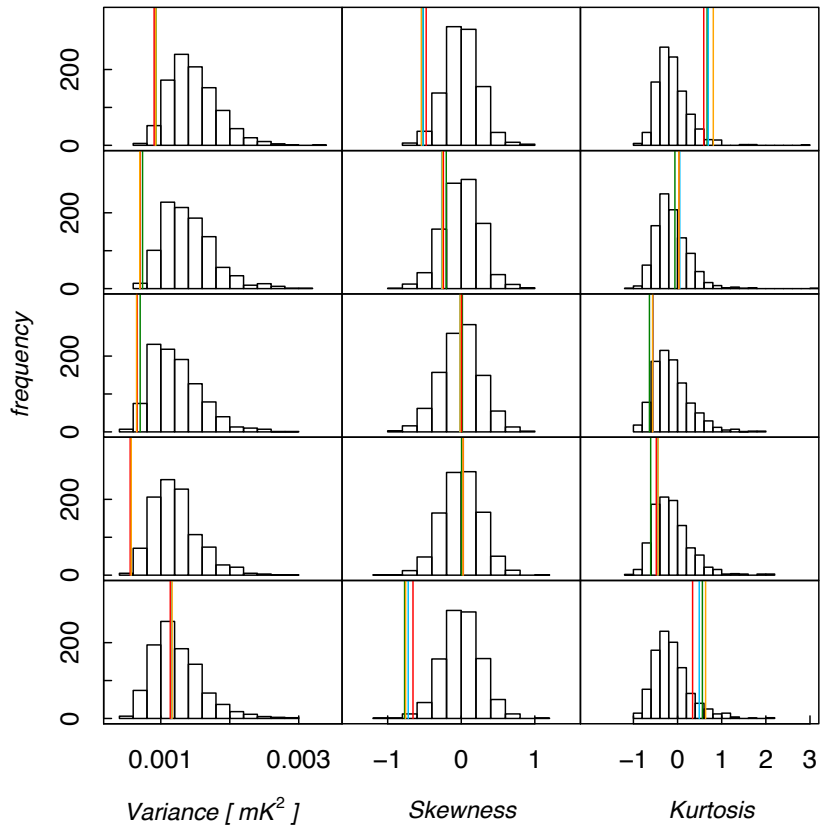

Fig. 21. Variance, skewness and kurtosis at $N_{side} = 16$, for the U73 mask, CL58, CL37, ecliptic North and ecliptic South (from top to bottom). The different lines represent the four component separation methods C-R (green), NILC (blue), SEVEM (red), and SMICA (orange).

The **low variance could be related to the largest scales anomalies**: notice that the cosmological parameter determination is mostly dominated by multipoles > 50, whilst the variance is more influenced by the largest scales.

Therefore, a mismatch between the data and the simulations at these scales will be reflected in the variance.

In fact, **after removal of the quadrupole and the octopole from the data, the three statistics are more compatible with the data**.

However, the **asymmetry problems persits**...

Isotropy and statistics of the CMB

Assessing the CMB anomalies

Low variance and hemispherical asymmetry

Table 20. Probabilities of obtaining values of the χ^2 statistic for the *Planck* fiducial model at least as large as the observed values of the statistic for the *Planck* maps with resolution parameter $N_{\rm side} = 64$ estimated using the C-R, NILC, SEVEM and SMICA methods.

	C-R	NILC	SEVEM	SMICA
	Two-point function			
Northern Ecliptic	0.935	0.924	0.927	0.932
Southern Ecliptic	0.633	0.599	0.639	0.592
	Pseudo-collapsed three-point function			
Northern Ecliptic	1.000	1.000	1.000	1.000
Southern Ecliptic	0.349	0.310	0.381	0.301
	Equilateral three-point function			
Northern Ecliptic	0.996	0.999	0.999	0.999
Southern Ecliptic	0.627	0.644	0.678	0.656
	Rhombic four-point function			
Northern Ecliptic	0.999	0.999	0.999	0.999
Southern Ecliptic	0.559	0.548	0.574	0.553

Similar asymmetry manifested by the N-point correlation functions.

The 2-pt indicates less power in the northern Ecliptic hemisphere.

The 3-pt and the 4-pt show less structure in the southern hemisphere.

Isotropy and statistics of the CMB

Assessing the CMB anomalies

Dipolar asymmetry

1st approach: Power asymmetry

It provides a **non-parametric approach to determine a dipolar anisotropy**:

1. Compute the power spectrum of the CMB from the cross-correlation of the hrhd maps (a la MASTER), into 768 discs centred in the N_{side} = 8 pixels

2. The 768 spectra are binned in 16 blocks of around 100 multipoles

3. The same is made with simulations. At each disc and at each block, the spectra are averaged, and referred to the mean power of the simulations (and normalized)

4. Each block has now an associated map at N_{side} = 8. The dipole direction of each map is estimated, and the alignment among all the dipole directions of the different blocks is identified as the dipole asymmetry (for isotropic skies, each block should have an independent dipole direction).

Isotropy and statistics of the CMB

Assessing the CMB anomalies

Dipolar asymmetry

1st approach: Power asymmetry

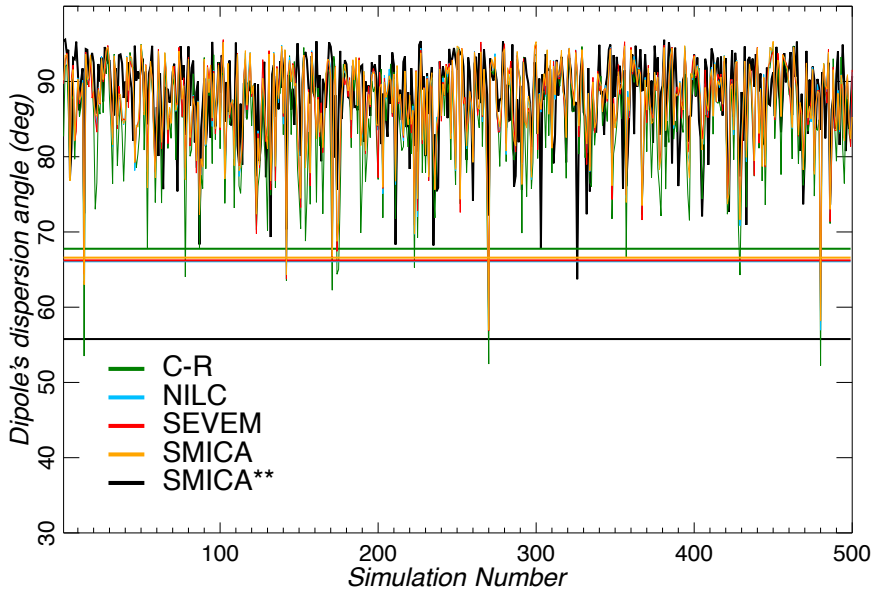

Fig. 26. Dispersion angles of the power spectra dipole directions, the mean of the differences of the dipole direction angles, up to ℓ_{max} = 1500, of the 500 FFP6 simulations compared to the *Planck* data with different foreground cleaning methods. All analyses, except `SMICA**`, are performed with the U73 mask. The `SMICA**` case is for `SMICA` data with the CS-SMICA89 mask.

Table 22. Summary of the power dipole directions on the sky, up to ℓ_{max} = 1500, as determined from maps of the power spectrum estimated from 768 22.5° radius discs and averaged over $\Delta\ell$ = 100 bins. The significance of the power asymmetry, shown in the last column, is quantified by the fraction of simulations that have smaller clustering of the dipole directions than the data. For the *Planck* analysis we used the 500 FFP6 simulations, while for *WMAP* we used 10000 Gaussian simulations.

Method	Mask	(l,b) [°]	θ^d_{mean} [°]	Frac. $\theta^{sim}_{mean} < \theta^d_{mean}$
`C-R`	U73	(231,−5)	67.8	11/500
`NILC`	U73	(223,−1)	66.1	4/500
`SEVEM`	U73	(224,2)	66.6	4/500
`SMICA`	U73	(225,1)	66.2	4/500

Isotropy and statistics of the CMB

Assessing the CMB anomalies

Dipolar asymmetry

2nd approach: Power asymmetry

Accounts for **a specific dipolar asymmetry (cosine modulation)**:

$$\mathbf{d} = (1 + A\,\boldsymbol{p}\cdot\boldsymbol{n})\mathbf{s}_{\rm iso} + \mathbf{n} \equiv \mathbf{M}\mathbf{s}_{\rm iso} + \mathbf{n}$$

data

Modulation amplitude

Modulation direction

isotropic field

noise

$$\mathcal{L}(A, \boldsymbol{p}, q, n) \propto \frac{e^{-\frac{1}{2}\boldsymbol{d}^{\rm T}\left(\mathrm{M^T SM + N} + \alpha \sum_i \boldsymbol{f}_i \boldsymbol{f}_i^{\rm T}\right)^{-1}\boldsymbol{d}}}{\sqrt{\left|\mathrm{M^T SM + N} + \alpha \sum_i \boldsymbol{f}_i \boldsymbol{f}_i^{\rm T}\right|}}.$$

Isotropy and statistics of the CMB

Assessing the CMB anomalies

Dipolar asymmetry

2nd approach: Power asymmetry

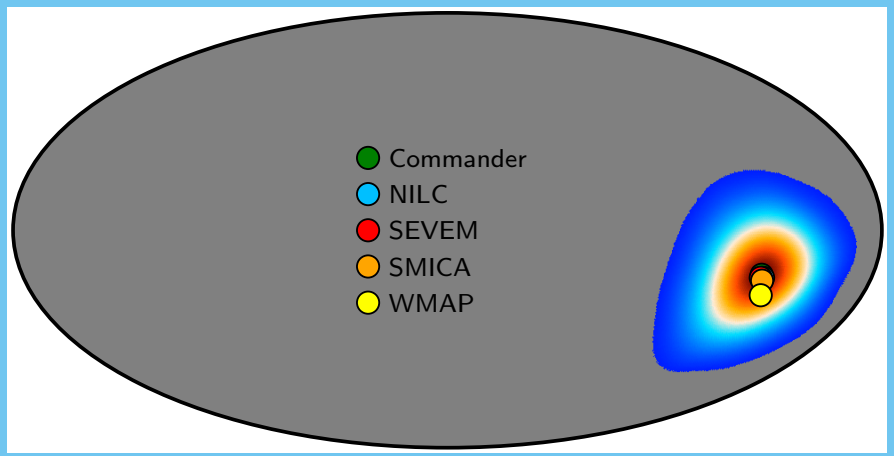

(l,b)[º] = (227, -15) +- 19

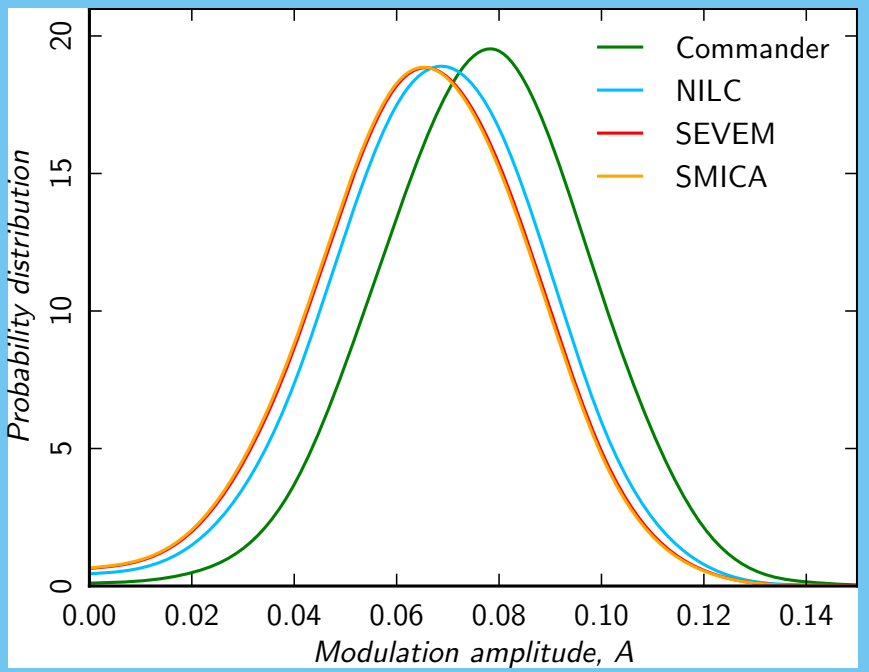

approx 3σ detection

Isotropy and statistics of the CMB

Generalized modulation

It relies on the **Bipolar Spherical Harmonic** (BipoSH) formalism, that is a **generalization of the angular power spectrum that captures isotropy violation**.

A simple model that results in the violation of statistical isotropy arises from the modulation of the CMB (but not necessary a cosine/dipolar modulation):

$$T(\boldsymbol{n}) = T_0(\boldsymbol{n})\,(1 + M(\boldsymbol{n}))$$

where the **modulation is assumed to be weak**, with quadratic terms neglected.

Isotropy and statistics of the CMB

Assessing the CMB anomalies

Generalized modulation

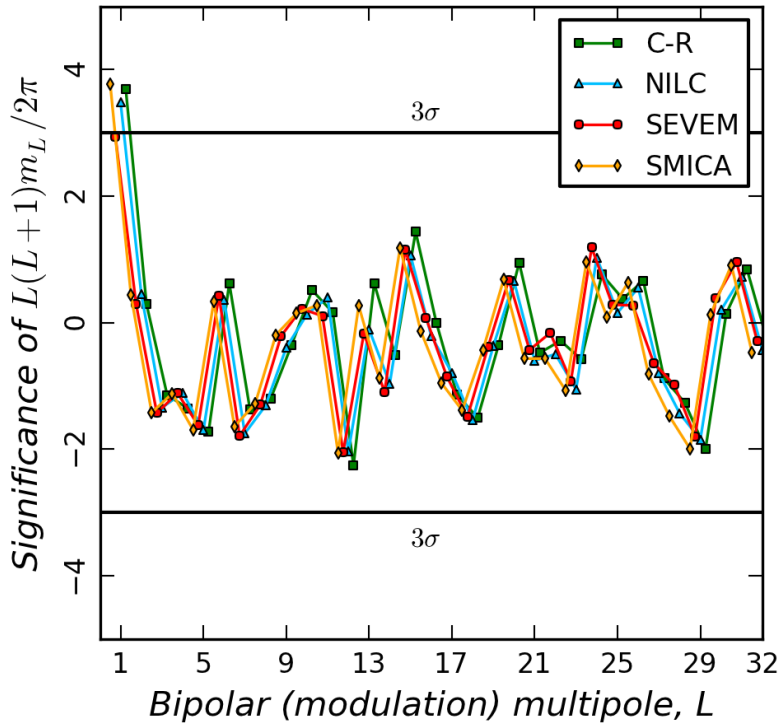

Fig. 32. The significance of the modulation power, $L(L+1)m_L/2\pi$, at bipolar multipoles L. The modulation spectra obtained from the four component separation maps (`C-R`, `NILC`, `SEVEM` and `SMICA`) are consistent with each other. Dipole ($L = 1$) modulation power is detected in all the spectra at a significance ranging from 3.7 to 2.9σ. The solid black lines denote the 3σ significance thresholds. There is no significant power detected at higher multipole of the modulation field $1 < L \leq 32$.

Table 24. This table lists the amplitude and direction of the dipole modulation in Galactic coordinates. The measured values of the dipole amplitude and direction are consistent for all maps. The corresponding dipole power for the `SMICA` map is seen at a detection significance of 3.7σ as shown in Fig. 32.

Map	Dipole Amplitude A	(l,b) [°] $(\sigma_l = 15.4, \sigma_b = 15.1)$
`C-R`	$0.072^{+0.01}_{-0.01}$	(218.9, −21.4)
`NILC`	$0.070^{+0.01}_{-0.01}$	(220.3 , −20.2)
`SEVEM`	$0.065^{+0.011}_{-0.011}$	(221.7 , −21.4)
`SMICA`	$0.073^{+0.01}_{-0.01}$	(217.5 , −20.2)

Only evidence of deviation for L=1, i.e, a dipolar modulation

Isotropy and statistics of the CMB

The Cold Spot

The **Cold Spot** was identified as an **anomalous cold and large spot in the southern hemisphere** of WMAP data (Vielva et al. 2004).

It accounts for a fraction of the anomalous kurtosis of the SMHW coefficients, but it appears more robust (against masking and foreground removal) when seen through the area of the wavelet coefficients above a given threshold.

Cold area $A_R^{-\nu} \equiv \#\{\omega_T(R,p) < -\nu\}$

Hot area $A_R^{+\nu} \equiv \#\{\omega_T(R,p) < +\nu\}$

Isotropy and statistics of the CMB

Assessing the CMB anomalies

The Cold Spot

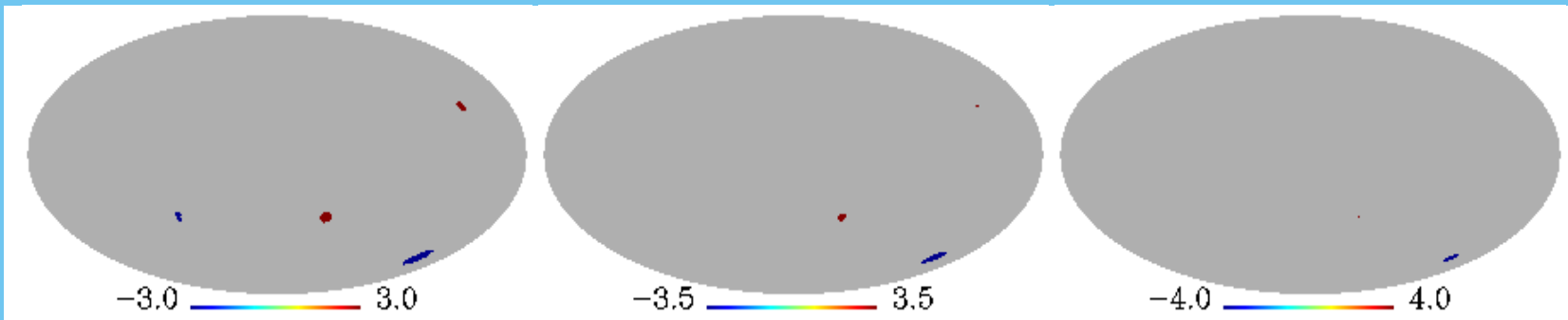

Fig. 37. SMHW coefficients at $R = 300$ arc minutes, and thresholds of 3.0σ (left), 3.5σ (middle), and 4.0σ (right). Results for the three masks considered in the analysis are shown: U73 mask (top), CG70 (middle) and CG60 (bottom).

Table 25. Upper tail probability (UTP, in %) associated to the cold (left) and hot (right) areas. Results are given for a $\nu > 4\sigma_R$ threshold and for the four *Planck* CMB maps. The three most significant scales associated to the Cold Spot are shown. Analysis performed on the exclusions masks associated with the U73 mask.

	Scale (R) [′]	C-R UTP (%)	NILC UTP (%)	SEVEM UTP (%)	SMICA UTP (%)
cold area	200	1.6	1.1	1.2	1.1
	250	0.3	0.3	0.3	0.3
	300	0.3	0.3	0.3	0.3
hot area	200	2.3	1.6	1.8	1.6
	250	2.7	2.2	2.4	2.2
	300	4.9	3.7	4.1	3.8

Isotropy and statistics of the CMB

Assessing the CMB anomalies

- Many features previously detected in WMAP data are also presented in Planck, **which rules out systematics as a source for them**.
- There is **evidence of statistical isotropy violation at least on large angular scales**.
- Moreover, **a dipolar power asymmetry may extend up to l=1500**, **whilst fits to a model containing a dipole modulation yield approx 3σ**.
- Evidence **of low-multipole spectrum departs from the Planck fiducial**
- Which is the origin of the anomalies?
  - Solar System emission as responsible for the large scale departures?
  - Coming from the local universe, via ISW ➔ hints of some tension reduction for some anomalies
  - Gravitational lensing or cosmic textures responsible for the Cold Spot?

Isotropy and statistics of the CMB

Of more interest (for us) would be that the anomalies are genuinely cosmological in origin.

In this respect, obvious candidate models include those with non-trivial topology. However, the dedicated **Planck XXVI paper** already shows no detection of such models (with the scale of the topology similar or larger to the diameter of the last-scattering surface.

However, this work also looks for consistency with an anisotropic Bianchi VIIh model (which already showed certain correlation with the WMAP data).

An **unphysical Bianchi VIIh model actually is preferred by the data**, which, ones subtracted from the data, provides **a new CMB map where most of the anomalies disappear** (multipole alignment, hemispherical asymmetry, the Cold Spot, …), **but not all of them** (low variance). We tested that, when this model is explored properly (i.e., coupled with the cosmological estimation coming from the power spectrum) there is no evidence of it.

Isotropy and statistics of the CMB

Assessing the CMB anomalies

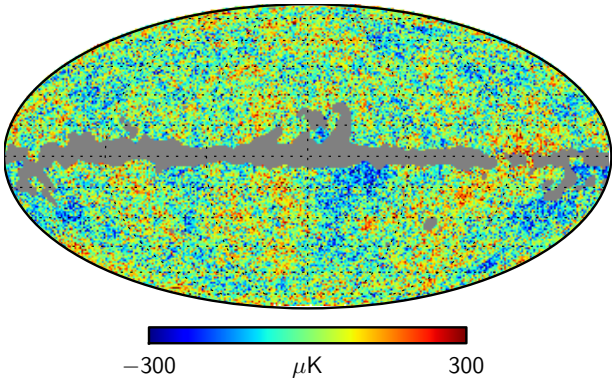

(a) SMICA CMB map.

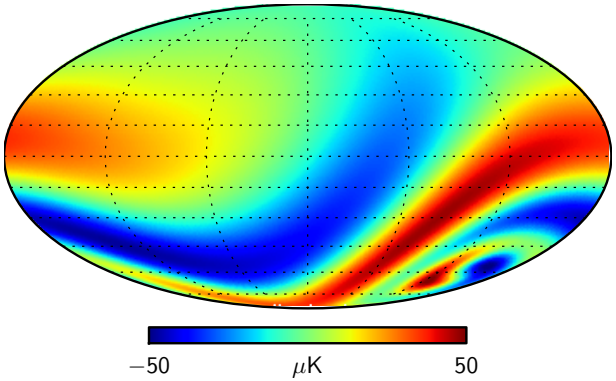

(b) Best-fit Bianchi VII_h map.

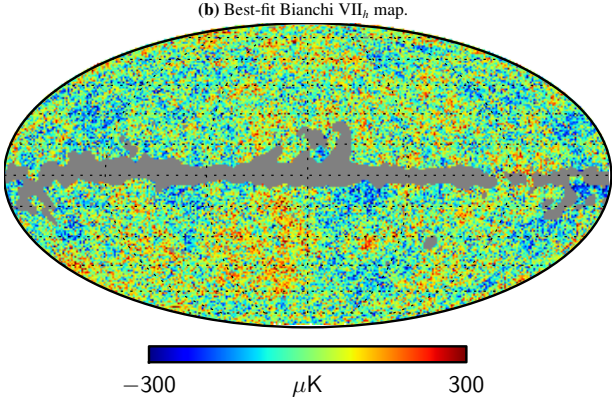

(c) SMICA CMB map with best-fit Bianchi component removed.

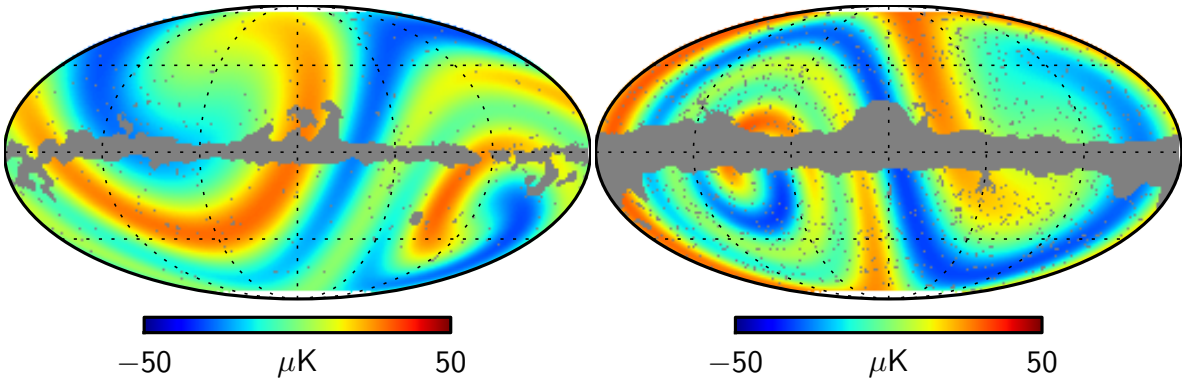

(a) SMICA **(b)** SEVEM

Fig. 23: Best-fit templates of left-handed open-coupled-Bianchi VII_h model recovered from *Planck* SMICA and SEVEM component-separated data. The Bayes factors for this model indicate that *Planck* data do not favour the inclusion of these Bianchi maps.

Table 3: Log-Bayes factor relative to equivalent ΛCDM model (positive favours Bianchi model).

Model	SMICA	SEVEM
Flat-decoupled-Bianchi (left-handed)	2.8 ± 0.1	1.5 ± 0.1
Flat-decoupled-Bianchi (right-handed)	0.5 ± 0.1	0.5 ± 0.1
Open-coupled-Bianchi (left-handed)	0.0 ± 0.1	0.0 ± 0.1
Open-coupled-Bianchi (right-handed)	−0.4 ± 0.1	−0.4 ± 0.1

The ISW-lensing bispectrum

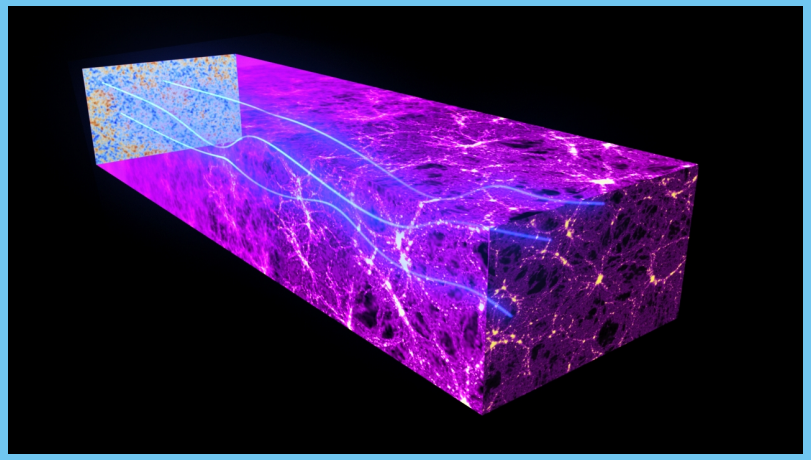

$$B^{m_1 m_2 m_3}_{\ell_1 \ell_2 \ell_3} \equiv \langle a_{\ell_1 m_1} a_{\ell_2 m_2} a_{\ell_3 m_3} \rangle = \langle a^{\rm P}_{\ell_1 m_1} a^{\rm L}_{\ell_2 m_2} a^{\rm ISW}_{\ell_3 m_3} \rangle + 5 \text{ perm.}$$

$$B^{m_1 m_2 m_3\,(\rm ISW-L)}_{\ell_1 \ell_2 \ell_3} = \mathcal{G}^{m_1 m_2 m_3}_{\ell_1 \ell_2 \ell_3} b^{\rm ISW-L}_{\ell_1 \ell_2 \ell_3}$$

$$b^{\rm ISW-L}_{\ell_1 \ell_2 \ell_3} = \frac{\ell_1(\ell_1+1) - \ell_2(\ell_2+1) + \ell_3(\ell_3+1)}{2} \times \tilde{C}^{\rm TT}_{\ell_1} C^{\rm T\phi}_{\ell_3} + (5 \text{ perm.})\,.$$

The **CMB lensing and the ISW are correlated**: both are caused by the matter gravitational potential. Planck provided the **first detection** of the ISW via this correlation.

Table 2. Amplitudes $A^{\rm T\phi}$, errors σ_A and significance levels of the non-Gaussianity due to the ISW effect, for all component separation algorithms (C-R, NILC, SEVEM, and SMICA) and all the estimators (potential reconstruction, KSW, binned, and modal). For the potential reconstruction case, an additional minimum variance (MV) map has been considered (see Planck Collaboration XVII 2013 for details).

Estimator		C-R		NILC		SEVEM		SMICA		MV	
$T\phi$	$\ell \geq 10$	0.52 ± 0.33	1.5	0.72 ± 0.30	2.4	0.58 ± 0.31	1.9	0.68 ± 0.30	2.3	0.78 ± 0.32	2.4
	$\ell \geq 2$	0.52 ± 0.32	1.6	0.75 ± 0.28	2.7	0.62 ± 0.29	2.1	0.70 ± 0.28	2.5		
KSW		0.75 ± 0.32	2.3	0.85 ± 0.32	2.7	0.68 ± 0.32	2.1	0.81 ± 0.31	2.6		
binned		0.80 ± 0.40	2.0	1.03 ± 0.37	2.8	0.83 ± 0.39	2.1	0.91 ± 0.37	2.5		
modal		0.68 ± 0.39	1.7	0.93 ± 0.37	2.5	0.60 ± 0.37	1.6	0.77 ± 0.37	2.1		

Constraints on primordial NG

The **ISW-lensing and the residual point sources bias the estimation of primordial bispectrum shapes with Planck data**:

Table 9. Results for the f_{NL} parameters of the primordial local, equilateral, and orthogonal shapes, determined by the KSW, binned and modal estimators from the SMICA, NILC, SEVEM, and C-R foreground-cleaned maps. Both independent single-shape results and results marginalized over the point source bispectrum and with the ISW-lensing bias subtracted are reported; error bars are 68% CL .

	Independent			ISW-lensing subtracted		
	KSW	Binned	Modal	KSW	Binned	Modal
SMICA						
Local	9.8 ± 5.8	9.2 ± 5.9	8.3 ± 5.9	**2.7 ± 5.8**	2.2 ± 5.9	1.6 ± 6.0
Equilateral	−37 ± 75	−20 ± 73	−20 ± 77	**−42 ± 75**	−25 ± 73	−20 ± 77
Orthogonal	−46 ± 39	−39 ± 41	−36 ± 41	**−25 ± 39**	−17 ± 41	−14 ± 42
NILC						
Local	11.6 ± 5.8	10.5 ± 5.8	9.4 ± 5.9	4.5 ± 5.8	3.6 ± 5.8	2.7 ± 6.0
Equilateral	−41 ± 76	−31 ± 73	−20 ± 76	−48 ± 76	−38 ± 73	−20 ± 78
Orthogonal	−74 ± 40	−62 ± 41	−60 ± 40	−53 ± 40	−41 ± 41	−37 ± 43
SEVEM						
Local	10.5 ± 5.9	10.1 ± 6.2	9.4 ± 6.0	3.4 ± 5.9	3.2 ± 6.2	2.6 ± 6.0
Equilateral	−32 ± 76	−21 ± 73	−13 ± 77	−36 ± 76	−25 ± 73	−13 ± 78
Orthogonal	−34 ± 40	−30 ± 42	−24 ± 42	−14 ± 40	−9 ± 42	−2 ± 42
C-R						
Local	12.4 ± 6.0	11.3 ± 5.9	10.9 ± 5.9	6.4 ± 6.0	5.5 ± 5.9	5.1 ± 5.9
Equilateral	−60 ± 79	−52 ± 74	−33 ± 78	−62 ± 79	−55 ± 74	−32 ± 78
Orthogonal	−76 ± 42	−60 ± 42	−63 ± 42	−57 ± 42	−41 ± 42	−42 ± 42

Constraints on cosmic strings

Current NG **constraints on cosmic strings are weaker than those imposed by the power spectrum**. Two major reasons: small number of simulations to characterize the NG statistics, and dealing with residual point sources.

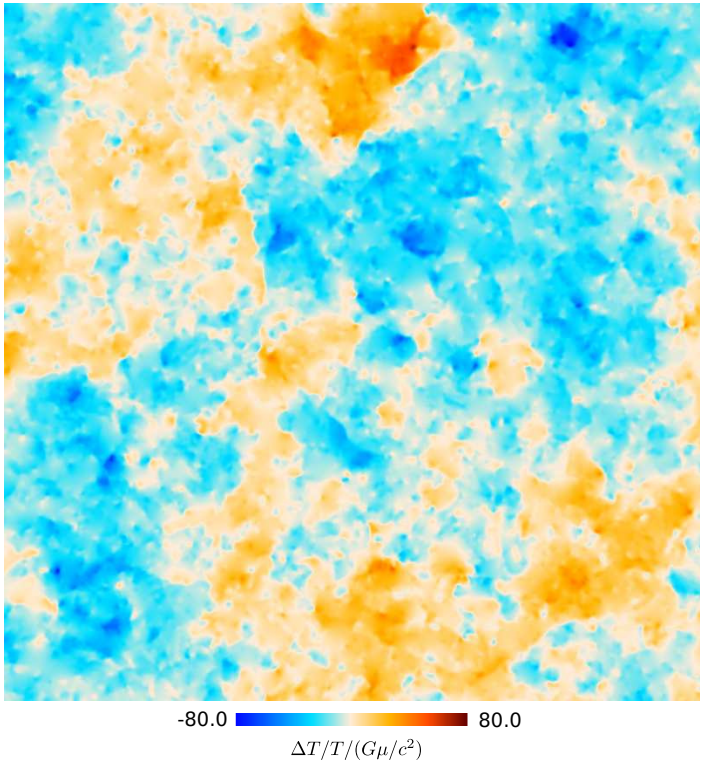

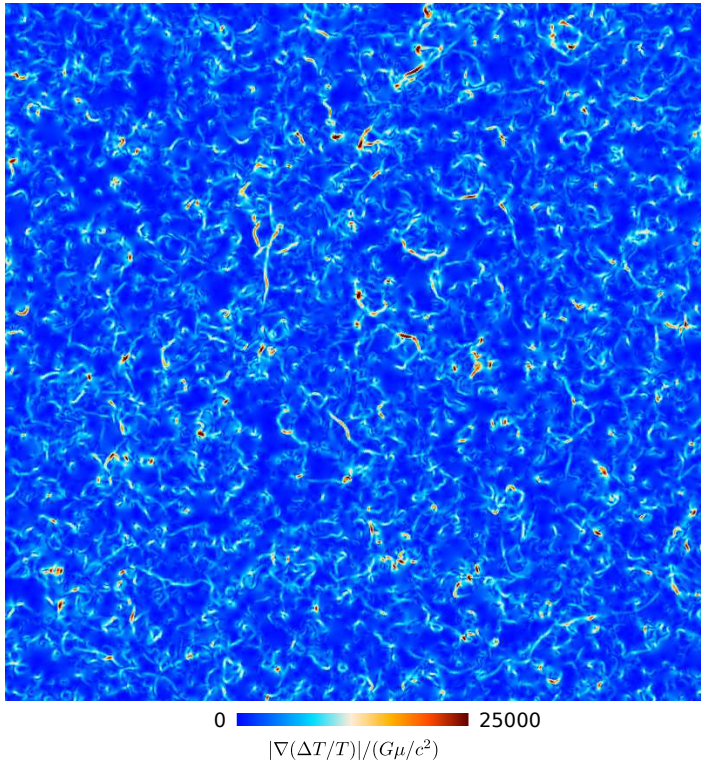

Fig. 7. A 20° gnomic projection patch extracted from the full sky map and zooming into string induced temperature steps (see Fig. 6). Applying the spherical gradient magnitude operator enhances the temperature steps, and thus the string locations, even more (right).

Constraints on cosmic strings

Current NG **constraints on cosmic strings are weaker than those imposed on the power spectrum**. Two major reasons: small number of simulations to characterize the NG statistics, and dealing with residual point sources.

From power spectrum analysis (95% CL)

Defect type	*Planck*+WP		*Planck*+WP+highL	
	f_{10}	$G\mu/c^2$	f_{10}	$G\mu/c^2$
NAMBU	0.015	1.5×10^{-7}	0.010	1.3×10^{-7}
AH-mimic	0.033	3.6×10^{-7}	0.034	3.7×10^{-7}
AH	0.028	3.2×10^{-7}	0.024	3.0×10^{-7}
SL Semilocal	0.043	11.0×10^{-7}	0.041	10.7×10^{-7}
TX Global texture	0.055	10.6×10^{-7}	0.054	10.5×10^{-7}

From NG analyses

Bispectrum $G\mu/c^2 < 8.8 \times 10^{-7}$ (95% CL)

Minkowski Functionals $G\mu/c^2 < 7.8 \times 10^{-7}$ (95% CL)

Conclusions

- **Expected NG signals detected**:
  - ISW-lensing (at 2.5σ)
  - Residual PS (at 4σ)

- **Only constraints on specific NG and anisotropic models**
  - primordial NG
  - cosmic strings
  - non-trival topology and anisotropic models

- **Some anomalies still present on the CMB data**
  - Low variance associated to a mismatch between the observed spectrum and the fiducial one
  - Somehow diminished alignment between the quadrupole and the octopole
  - Hemispherical asymmetry, also visible up to l=1500
  - Power asymmetry, notably in the form of a dipolar modulation
  - The Cold Spot

- Difficult interpretation of these anomalies… but, so far, they represent the only option to have some fun… we will see what polarization tell us

The scientific results here presented are a product of the Planck Collaboration, including individuals from more than 1000 scientific institutes in Europe, the USA and Canada

Planck is a project of the European Space Agency, with instruments provided by two scientific Consortia funded by ESA member states (in particular the lead countries: France and Italy) with contributions from NASA (USA), and telescope reflectors provided in a collaboration between ESA and a scientific Consortium led and funded by Denmark.